J. Membrane Biol. 201, 9–24 (2004)
DOI: 10.1007/s00232-004-0701-z

The Journal of
Membrane
Biology

Role of Arginine Residues on the S4 Segment of the *Bacillus halodurans* Na^+ Channel in Voltage-sensing

M. Chahine[1], S. Pilote[1], V. Pouliot[1], H. Takami[2], C. Sato[3]
[1]Research Centre, Laval Hospital, Sainte Foy, G1 V 4G5, and Department of Medicine, and Laval University, Quebec City, Quebec, Canada, G1K7P4
[2]Microbial Genome Research Group, Japan Marine Science & Technology Center, Yokosuka, Japan
[3]Neuroscience Research Institute and Biological Information Research Center (BIRC), National Institute of Advanced Industrial Science and Technology (AIST), Tsukuba, 305-8568, Japan

Received: 30 March 2004/Revised: 10 July 2004

Abstract. The one-domain voltage-gated sodium channel of *Bacillus halodurans* (NaChBac) is composed of six transmembrane segments (S1–S6) comprising a pore-forming region flanked by segments S5 and S6 and a voltage-sensing element composed of segment S4. To investigate the role of the S4 segment in NaChBac channel activation, we used the cysteine mutagenesis approach where the positive charges of single and multiple arginine (R) residues of the S4 segment were replaced by the neutrally charged amino acid cysteine (C). To determine whether it was the arginine residue itself or its positive charge that was involved in channel activation, arginine to lysine (R to K) mutations were constructed. Wild-type (WT) and mutant NaChBac channels were expressed in tsA201 cells and Na^+ currents were recorded using the whole-cell configuration of the patch-clamp technique. The current/voltage (*I-V*) and conductance/voltage (*G-V*) relationships steady-state inactivation (h_∞) and recovery from inactivation were evaluated to determine the effects of the S4 mutations on the biophysical properties of the NaChBac channel. R to C on the S4 segment resulted in a slowing of both activation and inactivation kinetics. Charge neutralization of arginine residues mostly resulted in a shift toward more positive potentials of *G-V* and h_∞ curves. The *G-V* curve shifts were associated with a decrease in slope, which may reflect a decrease in the gating charge involved in channel activation. Single neutralization of R114, R117, or R120 by C resulted in a very slow recovery from inactivation. Double neutralization of R111 and R129 confirmed the role of R111 in activation and suggested that R129 is most probably not part of the voltage sensor. Most of the R to K mutants retained WT-like current kinetics but exhibited an intermediate *G-V* curve, a steady-state inactivation shifted to more hyperpolarized potentials, and intermediate time constants of recovery from inactivation. This indicates that R, at several positions, plays an important role in channel activation. The data are consistent with the notion that the S4 is most probably the voltage sensor of the NaChBac channel and that both positive charges and the nature of the arginine residues are essential for channel activation.

Key words: Voltage-gated Na^+ channel — NaChBac — Gating charges — S4 segment — Voltage-sensor — *Bacillus halodurans*

Correspondence to: M. Chahine; email: mohamed.chahine@phc.ulaval.ca

Introduction

Ion channels are membrane proteins that control the movement of ions of excitable cells such as cardiac and skeletal myocytes and neurons (Armstrong and Hille, 1998; Hille, 2001). Voltage-gated ion channels contain regions that detect differences in the transmembrane potential of cell membranes and thus act as voltage sensors. Changes in cell membrane potential induce conformational changes, thereby closing or opening the channel. This opening and closing action of ion-selective channels controls the bidirectional flow of ions such as Na^+, Ca^{2+} and K^+ down their electrochemical gradients. Proteins of the ion channel superfamily possess a single α-subunit and at least one accessory β-subunit that modulate their expression levels and gating properties; (for reviews *see* Catterall, 1992, 2000; Fozzard & Hanck, 1996).

The α-subunits of sodium channels share a highly conserved structural motif (Strong, Chandy & Gutman, 1993). This motif consists of four homologous domains, each composed of six α-helices (S1–S6). The four domains fold together with the S5-S6 region of each domain, forming the ion permeation pathway. The S4 helix is the most conserved region in the ion channel family (Goldin, 2002). The hallmark of the S4 helix is its positively charged amino-acid residues separated by two hydrophobic amino-acids. It is this arrangement that is thought to play an important role in voltage sensing.

In the early fifties, Hodgkin and Huxley assumed that the opening of Na^+ and K^+ channels was due to the movement of charged gates (Hodgkin, Huxley & Katz, 1952). Stühmer et al. (1989), in pioneering research, mutated positively charged residues on the first cloned Na^+ channel from *Electrophorus electricus* (Noda et al., 1986) and directly implicated the positively charged residues on the S4 segment in channel activation and gating charge movement (Stühmer et al., 1989). Similar studies were carried out later on K^+ channels, confirming that gating charges associated with K^+ channel activation were correlated with the positively charged residues on the S4 segment (Liman et al., 1991; Papazian et al., 1991).

More recently, site-directed mutagenesis and chemically mediated cysteine mutagenesis showed that during depolarization, the S4 segment of $Na_v1.4$ moves to the extracellular space, thus explaining the transfer of one or two charges across the membrane (Chahine et al., 1994; Yang & Horn, 1995; Yang, George & Horn, 1996). Cysteine-modifying reagents exhibit extracellular accessibility to up to the fourth positively charged residue. These results are in agreement with the sliding helix model and suggest that the S4 helix rotates and translates toward the extracellular space (Catterall, 1986; Guy & Seetharamulu, 1986). However, another possibility is that if the S4 segment does not significantly translate to the extracellular space, a conformational change of the region surrounding the S4 helix would be necessary and this would explain the accessibility of cysteine-modifying reagents to certain buried S4 residues (Yang & Horn, 1995). The extent to which the S4 helix moves is still a subject of debate. Recent studies on *Shaker* K^+ channels suggest that a small 4 Å displacement could suffice to open these channels (Cha & Bezanilla, 1997; Cha et al., 1999; Gonzalez et al., 2001). This implies that the charge movement necessary for opening the channel is due more to rotation than to translation of the S4 helices.

Gating charge movement has been found to be kinetically synchronized to fluorescence, and this effect has been used to probe the real time dynamics of the voltage sensor of Na^+ channels (Glauner et al., 1999; Chanda & Bezanilla, 2002).

The recent crystallization of the six segments of KvAP, a K^+ channel from *Aeropyrum pernix*, revealed that the S4 segment may act as though it were a component of a voltage sensor "paddle." When the channel is closed, the voltage-sensor paddles are located along the intracellular surface on the periphery of channel protein and perpendicular to the ion permeation pathway (Jiang et al., 2003a,b). This is in contrast to the generally accepted idea that the S4 segment is oriented parallel to the ion permeation pathway and moves perpendicular to the membrane. In the paddle model, when the channel opens, the "paddles" move toward the extracellular space, applying torsion on the S4–S5 segment and opening the pore of the channel. However, this hypothesis has recently been challenged (Lainé et al., 2003) and it has been suggested that the N-terminal region of the S4 segment is close to the pore.

A prokaryotic Na^+-selective channel with a single domain was recently cloned from *Bacillus halodurans* and named NachBac (Ren et al., 2001) and most probably forms a homotetramer (Ren et al., 2003) with typical activation and inactivation kinetics. The one-domain Na^+ channels from bacteria will be of great value in elucidating the functions of different regions in mammalian voltage-gated Na^+ channels.

Here we cloned NachBac from *B. halodurans*; this alkaliphilic bacterium is the second member of *Bacillus* species to have its genome completely sequenced (Takami et al., 2000) and is the most thoroughly physiologically, biochemically and genetically characterized strain (Takami et al., 1999). We systematically neutralized single and multiple charges by cysteine mutagenesis of the six positively charged residues on the S4 region of the Na^+ channel (*see* Fig. 1) to understand how voltage sensing opens these channels. Charge-conserving mutants were also constructed to determine whether it is the positive charge or the arginine residue itself that mediates voltage sensing.

Our data show that charge neutralization resulted in a shift of steady-state activation (*G-V* curves) toward more depolarized voltages and a decreased slope. These data give a pivotal role to S4 arginine residues in the activation of the Na^+ channel.

Materials and Methods

Molecular Biology

Cloning of the NaChBac from Bacillus halodurans

A 1.1 kb DNA fragment containing the NaChBac channel was first amplified by polymerase chain reaction (PCR) from the chromosomal DNA of *B. halodurans* C-125 (Takami et al., 1999) with the following primer set: (5′-CTTTAGTCATGCGTACCCCT-

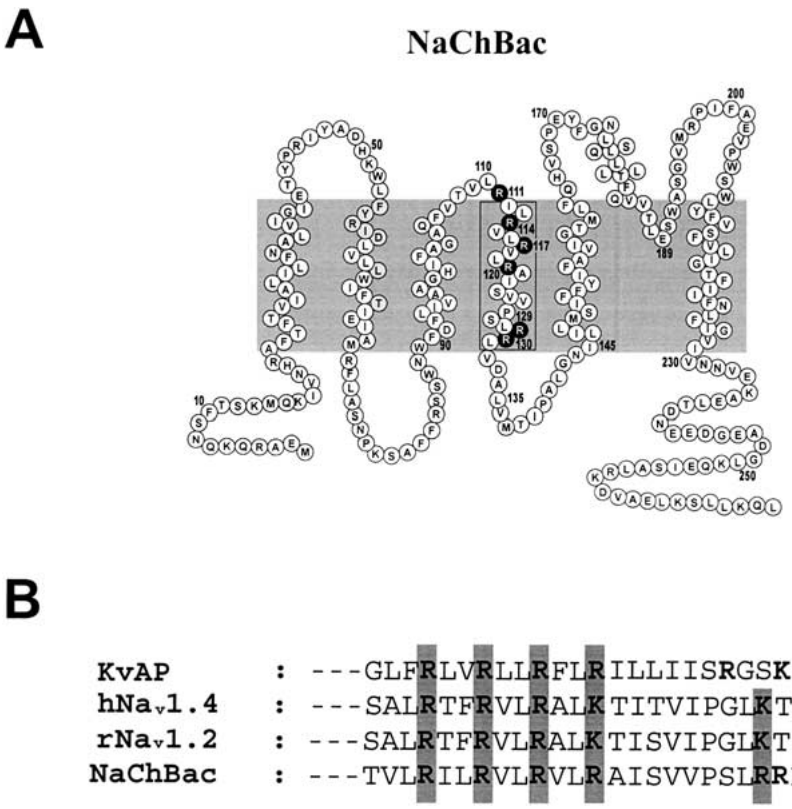

Fig. 1. Structure of the NaChBac and organization of the S4 segment. (*A*) Amino-acid sequence using the single-letter amino-acid code and schematic representation of the secondary structure of NaChBac. The S4 region with six arginine residues is highlighted. (*B*) Alignment of the amino-acid sequences using the single-letter amino-acid code of the S4 segment of NaChBac with S4 segments of the voltage-dependent K^+ channel from *Aeropyrum pernix* (KvAP), the rat brain Na^+ channel ($rNa_v1.2$) and the human skeletal muscle Na^+ channel ($hNa_v1.4$). DI-S4 was chosen because it displays higher homology with NaChBac-S4 than the other domains. Note the remarkable homology of the positively charged residues shown in bold.

CACCT-3′ and 5′-TGGTGCCGAGGAAACGGTTCA-3′). PCR was performed with a 9700 DNA thermal cycler (Perkin-Elmer, CT) under the following conditions: 25 cycles of 20 s at 96°C, 30 s at 58°C and 2 min at 72°C. An amplified PCR fragment was subcloned into the TA cloning vector, pCR2.1 (Invitrogen Japan, Tokyo, Japan). The insert was then further amplified by PCR and the amplified fragment was subcloned into pcDNA3.1 (Invitrogen, San Diego, CA). The entire gene was sequenced at the Laval University DNA sequencing facility in order to confirm the integrity of the gene product.

Recombinant DNA Constructions

The QuickChange™ site-directed mutagenesis kit from Stratagene (La Jolla, CA) was used according to the manufacturer's instructions. Mutant NaChBac channels were constructed using the following mutagenic sense and antisense primers. The mutated sites are underlined.

For R111C:

5′- CAA TTT GTG ACG GTT CTC TGT ATT TTA CGG GTT CTC AG -3′ and 5′- CT GAG AAC CCG TAA AAT ACA GAG AAC CGT CAC AAA TTG -3′

For R114C:

5′- CG GTT CTC CGT ATT TTA TGC GTT CTC AGG GTA CTA C -3′ and 5′- G TAG TAC CCT GAG AAC GCA TAA AAT ACG GAG AAC CG -3′

For R117C:

5′- GT ATT TTA CGG GTT CTC TGC GTA CTA CGG GCC ATC TC -3′ and 5′- GA GAT GGC CCG TAG TAC GCA GAG AAC CCG TAA AAT AC -3′

For R120C:

5′- CG GTT CTC AGG GTA CTA TGC GCC ATC TCA GTT GTT C -3′ and 5′- G AAC AAC TGA GAT GGC GCA TAG TAC CCT GAG AAC CG -3′

For R129C:

5′- CA GTT GTT CCA TCG TTG TGC AGG TTA GTT GAT GCG TTG -3′ and 5′- CAA CGC ATC AAC TAA CCT GCA CAA CGA TGG AAC AAC TG -3′

For R130C:

5′- GTT GTT CCA TCG TTG CGC TGC TTA GTT GAT GCG TTG GTG -3′ and 5′- CAC CAA CGC ATC AAC TAA GCA GCG CAA CGA TGG AAC AAC -3′

For R111 K:

5′- CAA TTT GTG ACG GTT CTC AAG ATT TTA CGG GTT CTC AG -3′ and 5′- CT GAG AAC CCG TAA AAT CTT GAG AAC CGT CAC AAA TTG -3′

For R114 K:

5′- CG GTT CTC CGT ATT TTA AAG GTT CTC AGG GTA CTA C -3′ and 5′- G TAG TAC CCT GAG AAC CTT TAA AAT ACG GAG AAC CG -3′

For R117 K:

5′- GT ATT TTA CGG GTT CTC AAG GTA CTA CGG GCC ATC TC -3′ and 5′- GA GAT GGC CCG TAG TAC CTT GAG AAC CCG TAA AAT AC -3′

For R120 K:

5′- CGG GTT CTC AGG GTA CTA AAG GCC ATC TCA GTT GTT C -3′ and 5′- G AAC AAC TGA GAT GGC CTT TAG TAC CCT GAG AAC CCG -3′

For R129 K:

5′- CA GTT GTT CCA TCG TTG AAG AGG TTA GTT GAT GCG TTG -3′ and 5′- CAA CGC ATC AAC TAA CCT CTT CAA CGA TGG AAC AAC TG -3′

For R130 K:

5′- GTT GTT CCA TCG TTG CGC AAG TTA GTT GAT GCG TTG GTG -3′ and 5′- CAC CAA CGC ATC AAC TAA CTT GCG CAA CGA TGG AAC AAC -3′

The R111C-R129C double mutant was constructed using the same primers as for R129C on an R111C mutant background. The presence of the mutation was confirmed by sequencing the entire

insert at the Laval University DNA sequencing facility. WT and mutant NaChBac DNA in the pcDNA3.1 (Invitrogen) construct were purified using Qiagen columns (Qiagen Inc., Chatsworth, CA, USA).

Transfection of the tsA201 Cell Line

TsA201 is a mammalian cell line derived from human embryonic kidney HEK 293 cells by stable transfection with SV40 large T antigen (Margolskee et al., 1993). The tsA201 cells were grown in high-glucose DMEM supplemented with FBS (10%), L-glutamine (2 mM), penicillin (100 U/ml) and streptomycin (10 mg/ml) (Gibco BRL Life Technologies, Burlington, ON, Canada) and incubated in a 5% CO_2 humidified atmosphere. The cells were transfected using the calcium phosphate method (Margolskee et al., 1993) with the following modification to facilitate the identification of individual transfected cells: a cotransfection with an expression plasmid for a lymphocyte surface antigen (CD8-a) was performed (Jurman et al., 1994). cDNA (10 μg) coding for WT or mutant NaChBac channels and 10 μg of CD8-a were used. For the patch-clamp experiments, cells were used two to three days post-transfection. The cells were incubated at room temperature in a medium containing anti-CD8-a-coated beads for 5 min (Dynabeads M-450 CD8-a). Unattached beads were removed by washing. The beads were prepared according to the manufacturer's instructions (Dynal Biotech Inc, Brown Beer, WI). Cells expressing surface CD 8-a fixed the beads and were visually distinguishable from nontransfected cells by light microscopy.

Patch-Clamp Method

Macroscopic Na^+ currents from tsA201 transfected cells were recorded using the whole-cell configuration of the patch-clamp technique (Hamill et al., 1981). Patch electrodes were made from 8161 Corning borosilicate glass and coated with Sylgard (Dow-Corning, Midland, MI) to minimize their capacitance. Patch-clamp recordings were made using low-resistance electrodes (<1 MΩ), and a routine series-resistance compensation by an Axopatch 200 amplifier (Axon Instruments, Foster City, CA) was performed to values > 80% to minimize voltage-clamp errors. Voltage-clamp command pulses were generated by a microcomputer using pCLAMP software v8.0 (Axon Instruments). Na^+ currents were filtered at 5 kHz, digitized at 10 kHz and stored on a microcomputer equipped with an AD converter (Digidata 1300, Axon Instruments). Data analysis was performed using a combination of pCLAMP software v9.0 (Axon Instruments), Microsoft Excel and SigmaPlot 2001 for Windows version 7.0 (SPSS Inc., Chicago, IL).

Solutions and Reagents

For whole-cell recordings, the patch pipette contained (in mM) 35 NaCl, 105 CsF, 10 EGTA and 10 Cs-HEPES. The pH was adjusted to 7.4 using 1 N CsOH. The bath solution contained (in mM) 150 NaCl, 2 KCl, 1.5 $CaCl_2$, 1 $MgCl_2$ 10 glucose and 10 Na-HEPES. The pH was adjusted to 7.4 with 1 N NaOH. For MTSET experiments, high-potassium solution contained (in mM) 100 K-aspartate, 50 KCl, 1.5 CaCl2,1 MgCl2, 10 glucose and 10 K-HEPES. The pH was adjusted to 7.4 with 1 N KOH. A −7 mV correction of the liquid junction potential between the patch pipette and the bath solutions was performed. While we did not observe any time-dependent shifts in the gating properties of WT and mutant Na^+ channels, the recordings were made 10 min after obtaining the whole-cell configuration in order to allow the current to stabilize and achieve adequate diffusion of the contents of the patch electrode. All the recordings were made in the following order: I/V curve, steady-state inactivation and recovery from inactivation. Due to the very slow inactivation and recovery from inactivation of NaChBac channel, in all protocols, cells were depolarized every 30 s. Experiments were performed at room temperature (22–23°C).

MTSET, [2-(Trimethylammonium)ethyl] methanethiosulfonate bromide was purchased from Toronto Research Chemicals (North York, Ontario, Canada). MTSET was dissolved in water and stored in aliquots on dry ice for the day to reduce freeze-and-thaw cycles.

Data Analyses

Given that the activation kinetics when resolved are generally sigmoid and not exponential, the half-time of activation ($t_{1/2}$) was used to study the activation kinetics. To study the inactivation kinetics, the decay of the Na^+ currents were fitted with a single exponential.

Na^+ channel conductance (G_{Na}) was calculated from currents obtained from the I/V protocol, using the equation $G_{Na} = I/(V-V_{Na})$, where V is the test potential and V_{Na} is the reversal potential for the Na^+ current calculated from the intercept of the linear interpolation of currents before and after reversal. The relationship between normalized G_{Na} and V was fitted using either one Boltzmann equation [$(G_{Na}/G_{Na,max} = 1/(\exp(V-V_{1/2})/k_v)$] or the sum of two Boltzmann equations [$G_{Na}/G_{Na,max} = (1-a)/(\exp(V-V_{1/2})/k_v) + a/(\exp(V-V'_{1/2})/k'_v)$] where $V_{1/2}$ and $V'_{1/2}$ are the potentials of 50% activation, k_v and k'_v are the limiting slope factors and a and $(1-a)$ are the relative weight factors. The steady-state inactivation curves or h_∞ were constructed using a double-pulse protocol with 4 s prepulse and 500 ms test pulse durations. Peak current amplitudes obtained from test pulses were normalized to their maximal values obtained at the holding potential of −140 mV or higher, depending on the mutation studied, and plotted versus the corresponding conditioning pulse. The fitting was performed using a Boltzmann equation [$I/I_{max} = 1/(\exp(V-V_{1/2})/k_v)$], where $V_{1/2}$ is the potential of 50% inactivation and k_v is the limiting slope factor.

The recovery from inactivation curves was constructed from data obtained using a double-pulse protocol with various interpulse intervals to allow recovery from inactivation. The conditioning pulse lasted 4 s. The fraction of Na^+ currents recovered from inactivation during the interpulse was fitted by a single exponential function [$I/I_0 = 1/(A\exp(-t/\tau_{rec.})$] where I_0 is the peak amplitude and I is the current amplitude during recovery of Na^+ current in response to the prepulse, t is the interpulse interval, $\tau_{rec.}$ is the time constant for the recovery from fast inactivation and A is the weighting factor.

Steady-state activation and inactivation parameters and the time constants of recovery from fast inactivation were determined using individual cells expressing mutant channels and were compared to the values obtained from WT channels. The values are reported in Table 1.

Statistical Analyses

Data are expressed as mean ± standard error of the mean (SEM). Where indicated, a Student's test was performed using statistical software in SigmaStat for Windows (SPSS Inc). Differences were deemed significant at $P < 0.05$.

Table 1. Activation, inactivation and recovery from inactivation parameters of wild-type and mutant NaChBac channels

	Activation				Inactivation		Recovery
	$V_{½}$ (mV)	Weighting Factor	(k_v) (mV)	z_m**	$V_{½}$ (mV)	(k_v) (mV)	τ (ms)
WT	−35.88 ± 1.10 (13)		10.13 ± 0.42 (13)	2.49	−71.10 ± 2.57 (8)	5.062 ± 0.18 (8)	495 ± 114 (3)
Charge neutralization							
R111C	−23.27 ± 2.54 (12)*		12.83 ± 0.81 (12)*	1.96	−70.73 ± 1.81 (5)	13.13 ± 0.80 (5)*	2902 ± 330 (3)*
R114C	−27.84 ± 4.18 (15)*	0.39 ± 0.02	15.67 ± 0.58 (15)*	1.61	−101.17 ± 2.96 (12)*	9.73 ± 0.73 (12)*	3268 ± 667 (6)*
	11.73 ± 2.02 (15)*	0.61 ± 0.02	6.56 ± 0.48 (15)*	3.84			
R117C	−32.53 ± 1.35 (8)		10.52 ± 0.70 (8)	2.40	−54.40 ± 1.98 (6)*	7.55 ± 1.10 (6)*	1690 ± 140 (4)*
R120C	10.93 ± 2.60 (8)*		6.20 ± 0.52 (8)*	4.06	−10.16 ± 1.44 (5)*	5.08 ± 0.43 (5)	714 ± 210 (3)
R129C	−3.40 ± 3.23 (8)*		12.38 ± 0.74 (8)*	2.04	−41.37 ± 3.68 (5)*	6.86 ± 0.38 (5)*	769 ± 82 (6)
R130C	−36.00 ± 3.08 (5)		10.62 ± 1.07 (5)	2.37	−62.95 ± 2.43 (3)	4.46 ± 0.51 (3)	776 ± 220 (3)
Charge conservation							
R111K	−39.10 ± 1.78 (9)†		12.87 ± 0.34 (9)*	1.97	−109.40 ± 1.52 (8)*†	5.30 ± 0.23 (8)†	885 ± 159 (4)†
R114K	−35.62 ± 4.54 (6)†		16.55 ± 1.28 (6)*	1.52	−90.78 ± 1.28 (5)*	5.41 ± 0.22 (5)†	656 ± 39 (4)†
R120K	−2.42 ± 1.85 (12)*†		14.93 ± 0.68 (12)*†	1.69	−89.91 ± 1.61 (7)*†	7.29 ± 0.25 (7)*†	828 ± 142 (3)
R129K	−7.23 ± 2.01 (8)*		15.67 ± 0.72 (8)*†	1.61	−88.08 ± 2.33 (8)*†	5.99 ± 0.18 (8)*†	425 ± 12 (5)†
R130K	−33.59 ± 2.91 (8)		9.73 ± 66 (8)	2.59	−78.19 ± 1.93 (6)†	5.14 ± 0.09 (6)	484 ± 69 (4)
Double neutralization							
R111CR129C	−21.00 ± 6.32 (6)*◇	0.48 ± 0.5 (6)	12.81 ± 1.45 (6)	1.97	−105.27 ± 4.97 (5)*£◇	12.65 ± 0.79 (5)*◇	2279 ± 260 (3)*◇
	16.12 ± 2.63 (6)*£◇	0.52 ± 0.5 (6)	4.98 ± 0.99 (6)*£◇	5.06			

*Significatively different from WT ($P < 0.05$).
†Significatively different from homologous RC ($P < 0.05$).
£Significatively different from R111C ($P < 0.05$).
◇Significatively different from R129C ($P < 0.05$).
**$z_m = RT/Fk_v$.

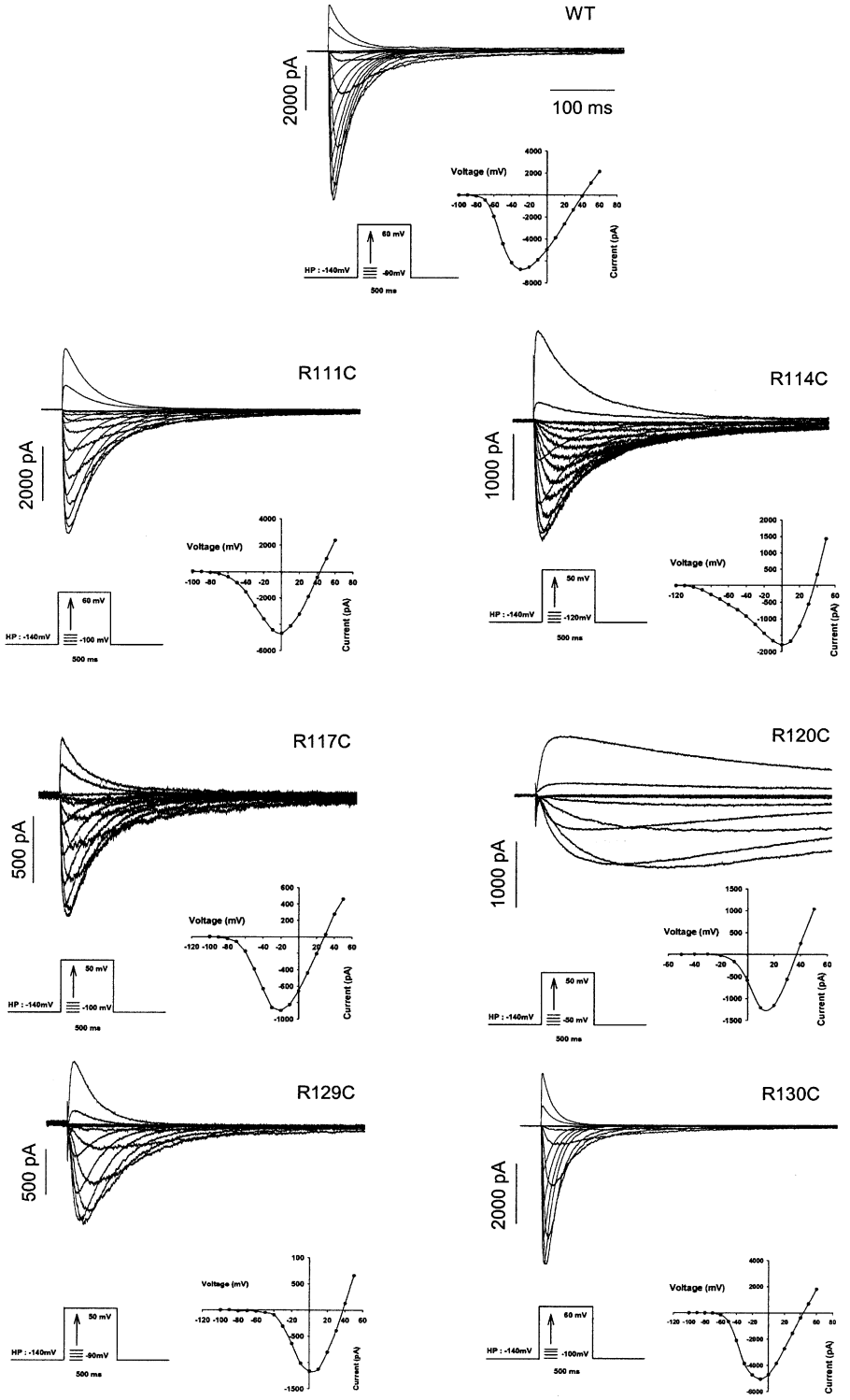

Fig. 2. Effects of neutralization of S4 charges on whole-cell macroscopic NaChBac currents. Representative whole-cell Na^+-current traces recorded from tsA201 cells expressing NaChBac-WT or S4 mutant Na^+ channels are shown. Na^+ currents, recorded at room temperature, were evoked by 4 s depolarizing pulses (only 500 ms are shown) starting at variable potentials, depending on the mutation. and rising to either 50 or 60 mV in 10 mV increments (*see* protocols in *insets*) from a –140 mV holding potential (*HP*), except for R114C, where the *HP* was –160 mV because of a large shift in the voltage at which the current appears. Note the low levels of current expression of the R114C mutant. The current-voltage relationship (*I-V*) is shown below each family of current traces. The maximum Na^+ current was plotted versus the applied voltage corresponding to each current trace shown for the NaChBac-WT or S4 mutant channels.

Results

Effects of Charge Neutralization of the S4 Segment Using Cysteine Mutagenesis

The S4 segment of the NaChBac contains positive charges, most of which are conserved, including

voltage-gated Na^+ channels from human skeletal muscle ($hNa_v1.4$), the rat brain ($rNa_v1.2$) and a voltage-dependent K^+ channel from *Aeropyrum pernix* (KvAP), (Fig. 1). The marked homology between NaChBac and the recently crystallized KvAP potassium channel suggests that the NaChBac S4 is likely to play a similar voltage-sensing role as the S4

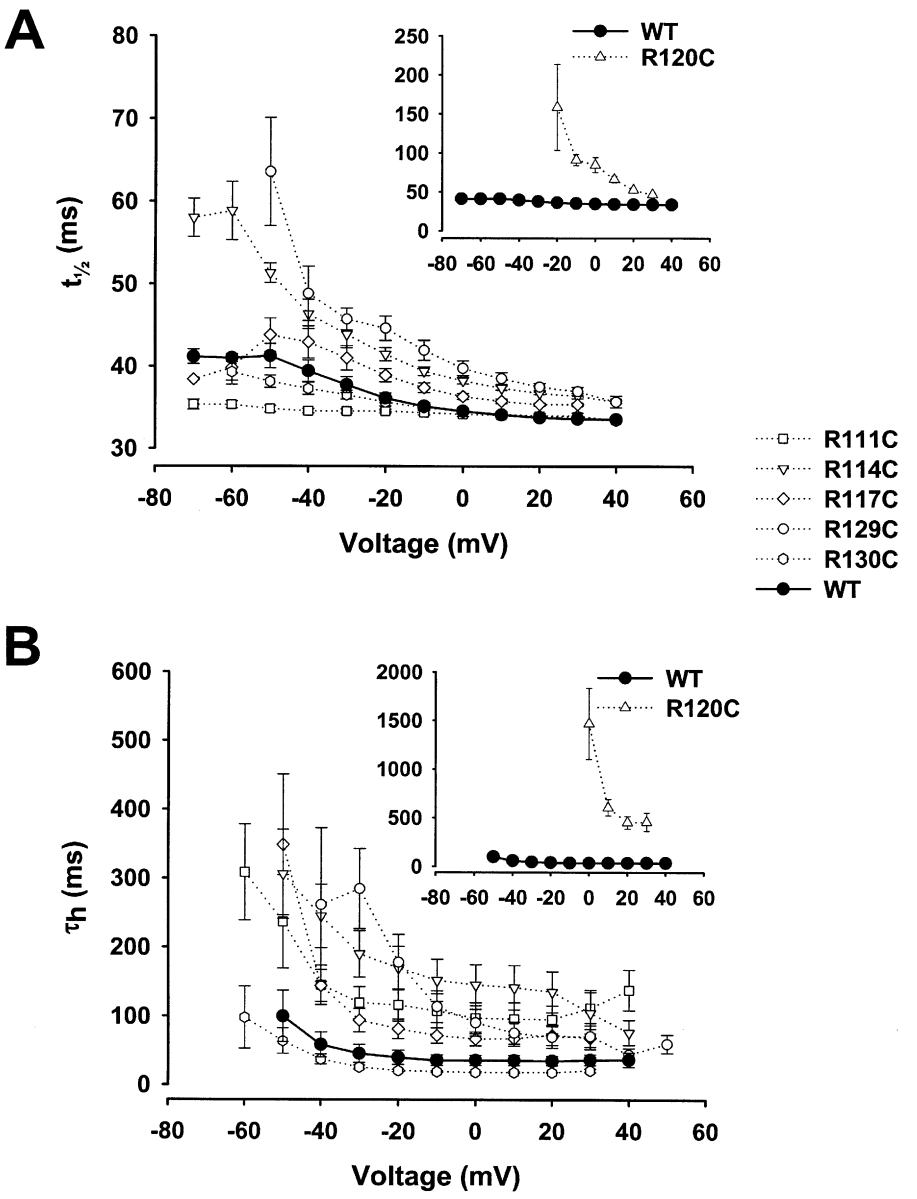

Fig. 3. Effects of neutralization of S4 charges on whole-cell macroscopic NaChBac current activation and inactivation kinetics. Voltage dependence of the time constants of activation (*A*) and inactivation (*B*). The $t_{1/2}$ of the rising Na^+ currents (activation) and the decay of the Na^+ currents (inactivation) fitted with single exponentials were determined. The values of the $t_{1/2}$ of activation and inactivation (τ_h) obtained were plotted versus the voltage. The values are expressed as means ± SEM for $n \geq 4$. In view of the fact that $t_{1/2}$ and τ_h were very slow for R120C, they are reported separately as an inset along with the values obtained from WT channels.

of the Kv type channels (Jiang et al., 2003a, b). In order to study the role of the six positively charged residues on the S4 segment of the NaChBac, they were neutralized by substituting each of them with cysteine, a neutral amino acid. Since this channel is devoid of cysteine, we were not concerned about cross-linking with endogenous cysteine. WT and mutant channels were then expressed in the tsA201 cell line and Na^+ currents were recorded in the whole-cell configuration.

Examples of Na^+-current traces from WT and mutant Na^+ channels are shown in Fig. 2. The threshold for activation of WT Na^+ currents was ~ -80 mV, while the peak current was −30 mV and reversed close to +37 mV (Fig. 2*A*), which is in agreement with the value predicted from the Nernst potential of Na^+ and consistent with the channel being selective for Na^+ ions.

As might be expected, the reversal potentials of all S4 charge-neutralizing mutant channels were not affected (Fig. 2), suggesting that these mutations do not disturb the selectivity of the channel.

The R111C and R117C S4 mutant channels activated at a potential similar to the WT channel (−80 mV). The R114C mutant channel activated at more hyperpolarized voltages (Fig. 2). The R111C and R114C currents reached a peak at 0 mV. The *I-V* curves from R120C and 129C (Fig. 2) were shifted to more depolarized voltages, reaching a peak at +20 mV and 0 mV, respectively. Na^+ currents from the R130C mutant were activated at more depolarized voltages (−60 mV) and reached a maximum at −10 mV.

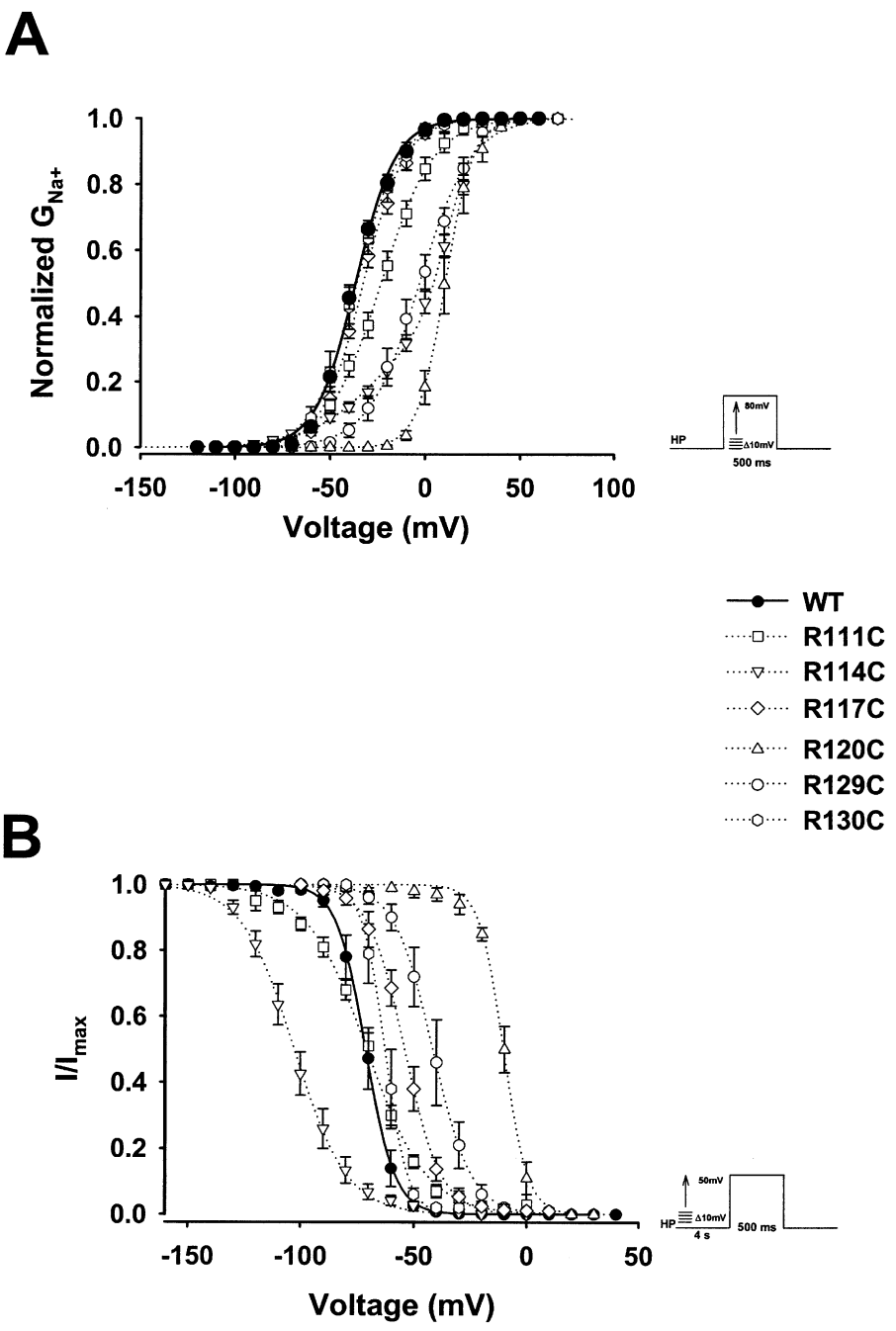

Fig. 4. Effects of neutralization of S4 charges on steady-state activation (*G-V*) and steady-state inactivation (h_∞). Voltage-dependence of normalized conductance (*G-V*) for NaChBac WT and S4 mutant Na^+ channels (*A*). The symbols correspond to normalized conductance values and the lines are the Boltzmann distribution fittings for the data points ($V_{1/2}$ and k_v parameters are shown in Table 1). (*B*) Steady-state availability (h_∞) relations for NaChBac WT and mutant channels. The symbols correspond to normalized (I/I_{max}) current values and the lines are the Boltzmann distribution fittings for the data points ($V_{1/2}$ and k_v parameters are shown in Table 1).

The voltage-dependence of activation and inactivation was studied by determining the half-time of activation ($t_{1/2}$) and by fitting the current decay (inactivation), using single exponentials of the current traces to obtain the time constant of inactivation (τ_h). One exponential was sufficient to describe the kinetics of inactivation. The time constants were then plotted versus voltage, as indicated on Fig. 3. The neutralization of positively charged residues on the S4 segment clearly resulted in a slowing of Na^+-channel activation and inactivation kinetics, as shown by the increase in the $t_{1/2}$ (Fig. 3*A*) and τ_h in the majority of the mutants (Fig. 3B). The greatest effect was observed with the R120C mutant, where dramatic changes in $t_{1/2}$ and τ_h were observed (*see* Figs. 3*A* and *B* insets). However, neutralization of the arginine residue at position 130, the last positively charged residue, resulted in an opposite effect with more rapid activation and inactivation kinetics (Fig. 3). The changes in $t_{1/2}$ and τ_h correlated, except for the R111C mutant, which exhibited slow current decay kinetics but faster rising current kinetics.

To assess changes in gating charges, *G-V* curves were constructed for each mutant and the data were

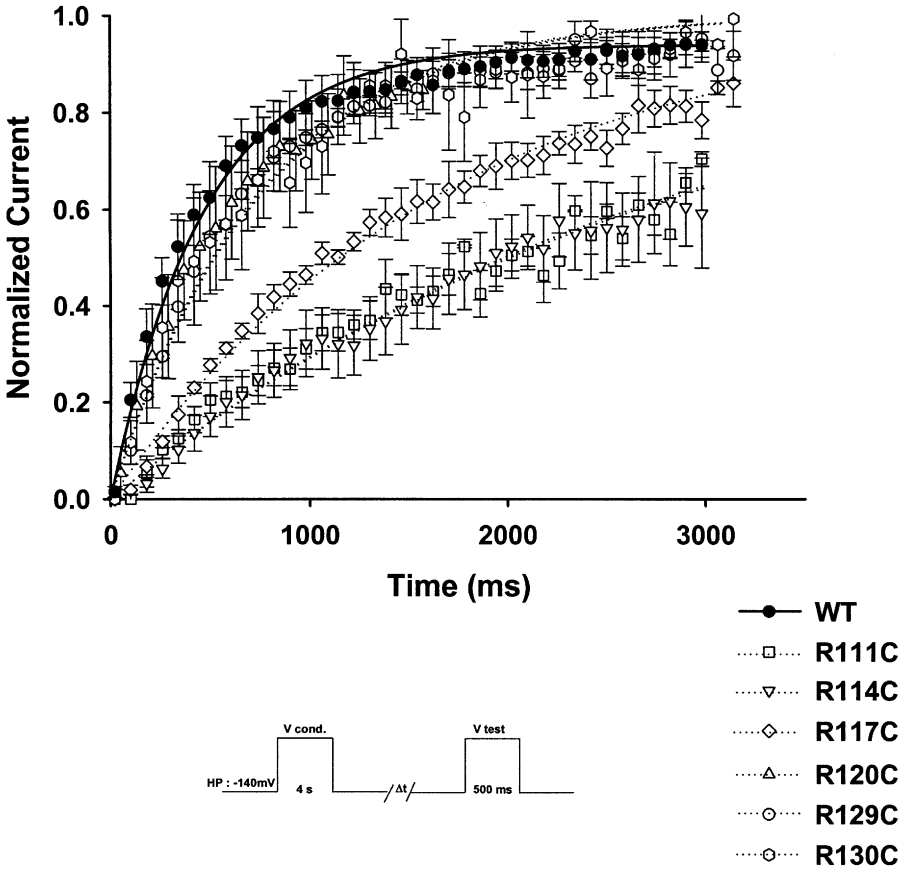

Fig. 5. Effects of neutralization of S4 charges on recovery from inactivation. The recovery from fast inactivation was studied at a holding potential of –140 mV for NaChBac WT and S4 mutant Na^+ channels. The symbols correspond to normalized (I/I_{max}) current values and the lines are single exponential fittings to the data points. The time constants of recovery from inactivation for NaChBac-WT and S4 mutant Na^+ channels are reported in Table 1. The inset shows a schematic representation of the protocol used to study recovery from fast inactivation.

fitted with a Boltzmann function that enabled us to estimate two important variables: midpoint potentials ($V_{1/2}$) and the slope factor (k_v). These parameters for WT and each mutation are summarized in Table 1. We estimated the apparent gating charge value (z) from the slope factor of the *G-V* curve (Table 1). Dramatic changes of the *G-V* curve were observed with the R111C, R114C, R120C and R129C mutants, pointing to major changes in activation (Fig. 4*A*). In particular, neutralizing positively charged residues in the S4 region resulted in a shift of *G-V* curves to more depolarized potentials (Table 1). These shifts in the *G-V* curve were accompanied by a less steep slope conductance. The *G-V* curve of the R114C mutant exhibited complex behavior and was fit with a sum of two Boltzmann functions (Fig. 4*A*, *filled, down-pointing triangles*). R120C exhibited the strongest shift of the *G-V* curve (45 mV toward more depolarizing potentials), with the slope being even steeper: $k_v = 6.2 \pm 0.52$ versus $k_v = 10.13 \pm 0.42$ for WT channels (Fig. 4*A*, upward, closed triangles, and Table 1).

Steady-state inactivation (h_∞) was also studied on WT and mutant Na^+ channels, using a two-pulse protocol with a 4 s prepulse (Fig. 4*B*). Steady-state inactivation exhibited shifts that correlated with those observed with *G-V* curves, except for the R114C mutant, which exhibited a shift in the opposite direction. These shifts were reflected in the values obtained from Boltzmann function fits, with both midpoint of inactivation ($V_{1/2}$) and slope factors (k_v) being less steep (Table 1).

The recovery from fast inactivation was studied using a two-pulse protocol. The test voltages were set at the voltage that generated a maximum current. The 4 s conditioning pulse was followed by a variable duration pulse (Δt) at −140 mV and then a 100 ms test pulse (Fig. 5). The time constants of recovery from fast inactivation (τ_{rec}) were obtained by fitting the amplitude of the Na^+ currents obtained during the recovery times using a single exponential function. The cysteine substitutions of R111, R114 and R117 generated slow time constants of recovery, with R111C and R114C exhibiting the slowest time constants of recovery, from inactivation (τ_{rec}) (2902 ± 330 ms for R111C and 3268 ± 677 ms for R114C versus 495 ± 114 ms for WT channels), whereas changes in the τ_{rec} of R120C, R129C and R130C were not statistically significant from that of the WT channel (Table 1).

The Effects of Multiple Charge Neutralization on the S4 Segment

We also neutralized multiple positive charges to study the contribution of combined charge neutralization on channel activation and inactivation kinetics

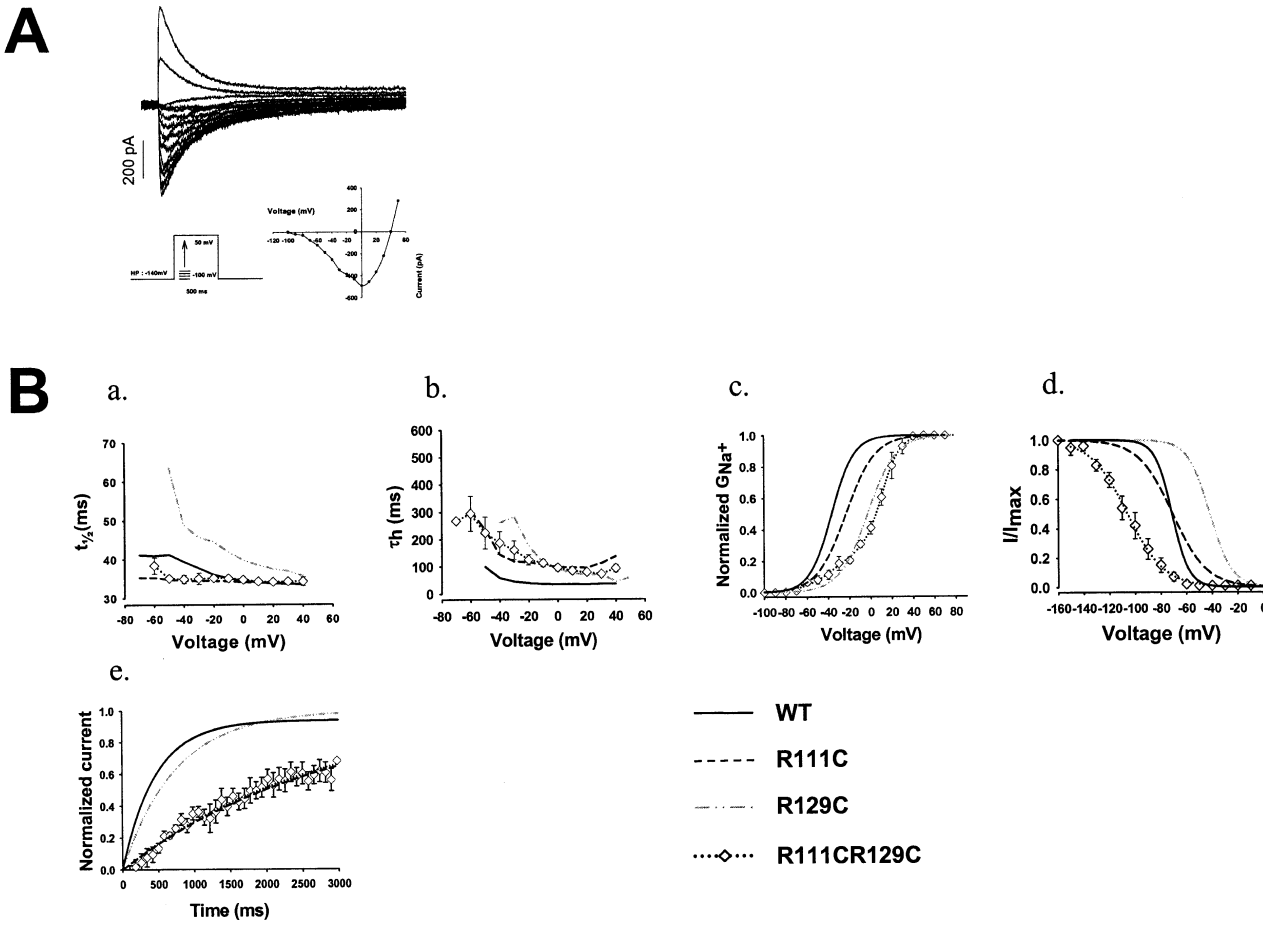

Fig. 6. Effects of a double-charge neutralization (R111C-R129C) on whole-cell macroscopic NaChBac activation and inactivation kinetics, steady-state activation (*G-V*), steady-state inactivation (h_∞) and recovery from inactivation. (*A*) Whole-cell Na^+-current traces recorded from tsA201 cells expressing R111C-R129C S4 double-mutant Na^+ channels. Na^+ currents were evoked by 4 s depolarizing pulses (only 500 ms are shown) starting at –100 mV in 10 mV increments (*see* protocol in inset) from a holding potential (*HP*) of –140 mV. The current-voltage relationships (*I-V*), where the maximum Na^+ current was plotted versus the applied voltage, are shown below the family of whole-cell Na^+-current traces. (*B*) Voltage-dependence of $t_{1/2}$ of activation (*a*) and inactivation (τ_h) (*b*). The rising Na^+ currents (activation) and the decay of Na^+ currents (inactivation) were fitted with single exponentials and the values of the time constants of activation and inactivation ($t_{1/2}$ and τ_h, respectively) were plotted versus voltage. Values are expressed as means ± SEM for $n \geq 5$. (*B-c*) Normalized conductance versus voltage (*G-V*) relations for NaChBac WT and S4 double neutralization mutant Na^+ channels. The symbols are normalized conductance values and the lines are Boltzmann fits to the data points (the $V_{1/2}$ and k_v parameters are reported in Tablel 1). (*B-d*) Steady-state availability (h_∞) relations for NaChBac WT and double neutralization mutant channels. The symbols are normalized (I/I_{max}) current values and the solid lines are Boltzmann fits to the data points (the $V_{1/2}$ and k_v parameters are reported in Table 1). (*B-e*) The recovery from fast inactivation was studied at a holding potential of –120 mV for NaChBac WT and S4 double neutralization mutant Na^+ channels. The symbols are normalized (I/I_{max}) current values and the solid lines are single-exponential fits to the data points. The time constants of recovery from inactivation for NaChBac-WT and S4 double neutralization mutant Na^+ channels are reported in Table 1.

(Fig. 6). These data were compared with data from point neutralization and WT channels to determine whether the change in charge had a cumulative effect on the biophysical properties of the channels. Like the single substitutions, the reversal potential was in agreement with the value predicted from the Nernst potential of Na^+ ($\sim +37$ mV), suggesting that the double mutant did not alter Na^+ selectivity. The double mutant R111C-R114C did not generate Na^+ currents. When R111C and R129C were combined, the time constants of activation were faster at −60 and −50 mV and similar to the WT and the R111C mutant from −40 to +40 mV (Fig. 6*B-a*). However, the time constants of inactivation were slow and displayed similarities to the R111C mutant channels (Fig. 6*B-b*). The *G-V* curve of the double mutant exhibited complex behavior with the sum of two Boltzmann functions, being intermediate between R111C and R129C at low voltage (−100 to −20 mV) but similar to the R129C mutant at voltages more

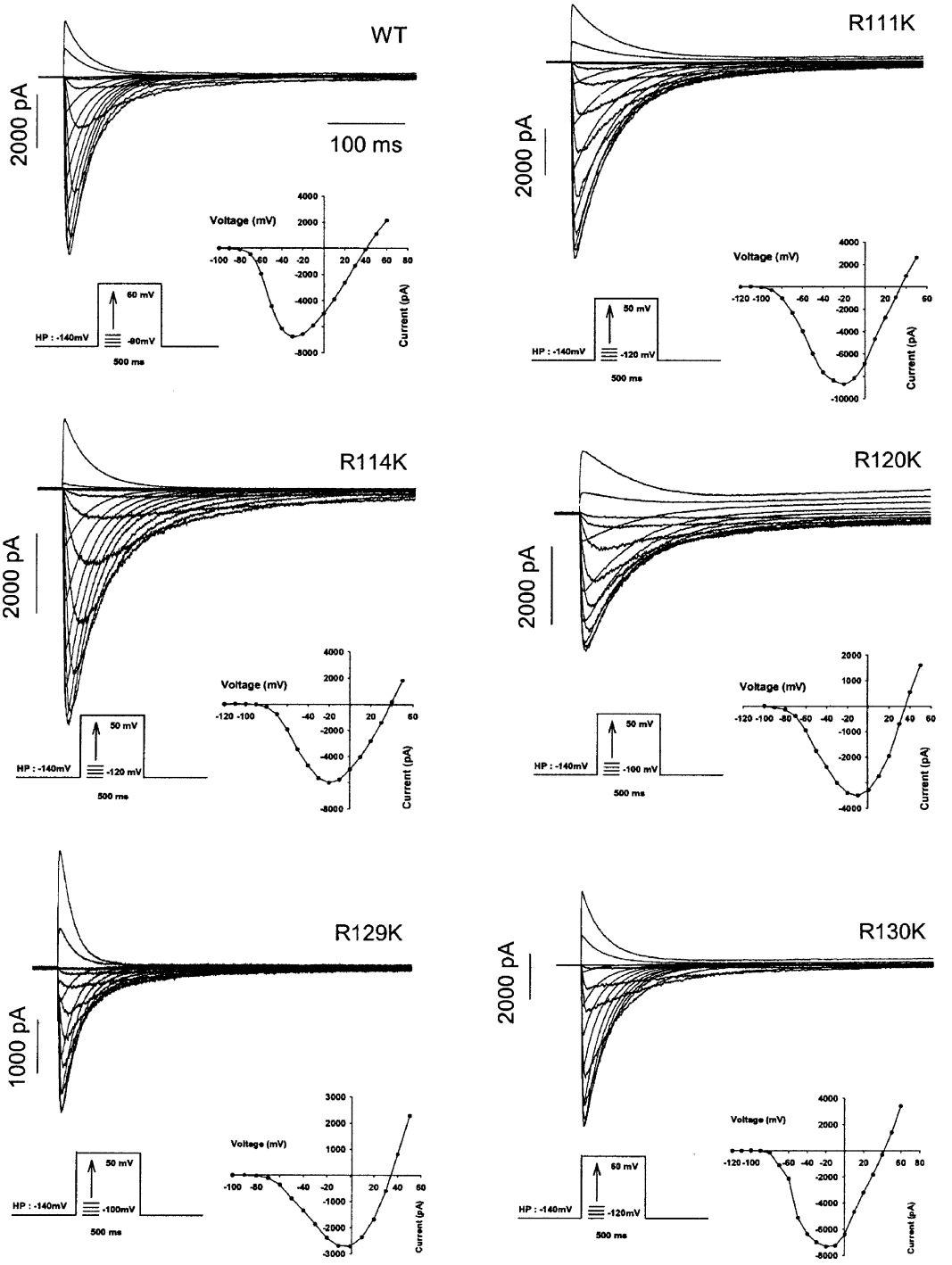

Fig. 7. Effects of S4 charge-conservative mutations on whole-cell macroscopic S4 NaChBac Na^+ currents: Representative whole-cell Na^+ current traces recorded from tsA201 cells expressing charge-conservative S4 mutant Na^+ channels are shown. Na^+ currents were evoked by 4 s depolarizing pulses (only 500 ms are shown) at variable potentials, depending on the mutation, from either –100 mV or –120 mV to either 50 or 60 mV in 10 mV increments (*see* protocol in insets) from a holding potential (*HP*) of –140 mV. The current voltage relationships (*I-V*), where the maximum Na^+ current was plotted versus the applied voltage corresponding to each current trace of charge-conservative mutants, are shown in the insets below each family of current traces.

positive than −20 mV (Fig. 6*B-c* and Table 1 for *G-V* parameters).

Steady-state inactivation was shifted toward more hyperpolarized voltages for the double mutant (Fig. 6*B-d* and Table 1 for h_∞ parameters). This shift could result from the very slow recovery from fast inactivation observed with the double mutant relative to the WT channels. The time constant of recovery

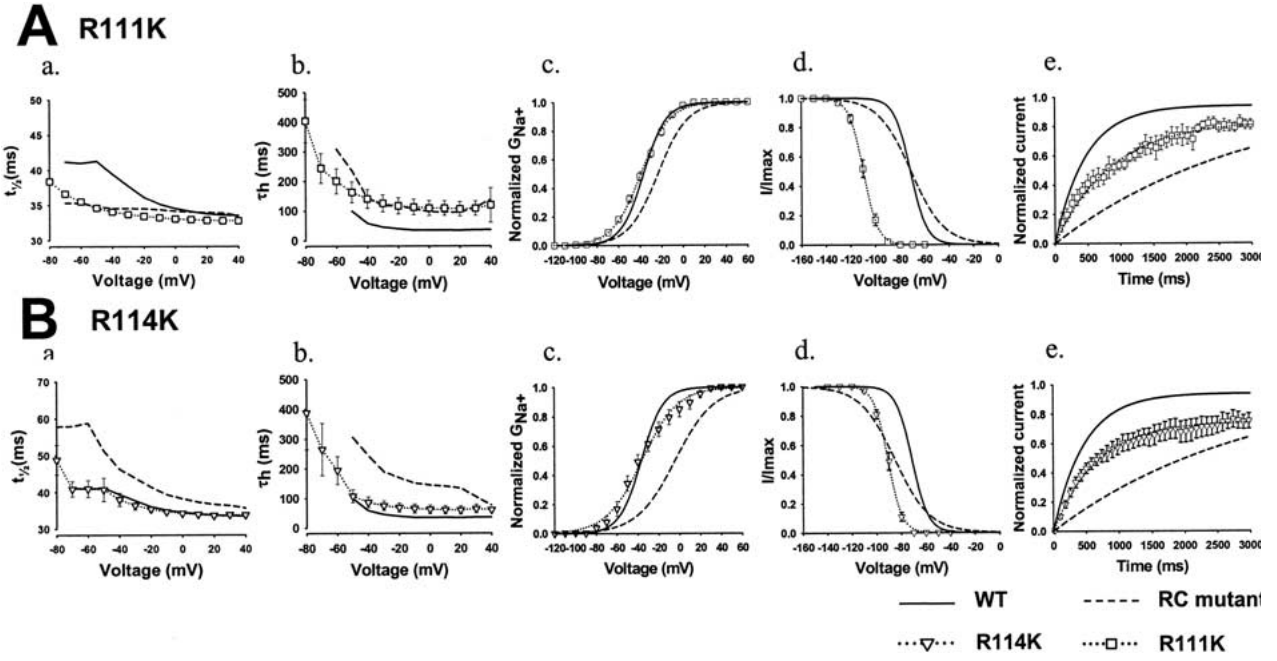

Fig. 8. Effects of charge-conservative mutations in S4 (R111K and R114K) on sodium-current activation and inactivation kinetics, steady-state activation (*G-V*) and inactivation h_∞ and recovery from inactivation. Voltage-dependence of $t_{1/2}$ of activation (*A-a*) and inactivation (τ_h) (*A-b*), normalized conductance versus voltage (*G-V*) (*A-c*), steady-state availability (h_∞) (*A-d*) and recovery from fast inactivation (*A-e*) for R111K mutant Na^+ channels at a holding potential of –140 mV. For comparison, plots for WT and R111C are shown on the same graphs. Voltage-dependence of $t_{1/2}$ of activation (*B-a*) and inactivation (τ_h) (*B-b*), normalized conductance versus voltage (*G-V*) (*B-c*), steady-state availability (h_∞) (*B-d*) and recovery from fast inactivation (*B-e*) for R114K mutant Na^+ channels at a holding potential of –140 mV. For comparison, plots for WT and R114C are shown on the same graphs. For *G-V* and h_∞, the symbols are normalized values and the lines are single Boltzmann fits to the data points.

obtained from a single-exponential fit was very slow and comparable to that observed for R111C (Table 1).

Effects of Conserving Positive Charges on the S4 Segment

In the R to K substitution experiments, no R to K mutants exhibited altered Na^+ selectivity, as seen by their reversal potentials, which were similar to that of the WT, and the agreement with the value predicted from the Nernst potential of Na^+ ($\sim +37$ mV) (Fig. 7). Mutant R117 K did not generate Na^+ currents. Charge conservation did not result in complete preservation of the five parameters studied (Fig. 7, Fig. 8 and Table 1), as exemplified by mutant R120 K (Fig. 9*A*). R120 K displayed Na^+ current activation (Fig. 8*A-a*) and inactivation (Fig. 9*A-b*) kinetics that were similar to those of WT channels. The *G-V* curve was intermediate between the WT and the R120C mutant (Fig. 9*A-c*). Steady-state inactivation exhibited a dramatic shift to more hyperpolarized voltages (Fig. 9*A-d*). However, as with R120C, the recovery from inactivation was the same as that of the WT channels (Fig. 9*A-e*).

The effect of charge conservation at position 130 further illustrates that the positive charge on the arginine residue and not the arginine as such plays an important role at this site. Indeed, when the R residue at position 130 was substituted with a K to form the R130 K mutant, the time constants of activation and inactivation were indistinguishable from WT (Fig. 9*C-a* and *b*). That the *G-V* curves were the same as those of the WT and R130C mutant (Fig. 9*C-c*) is supported by the kinetics of activation. In fact, the $V_{1/2}$ value of R130 K was not significantly different from those of R130C and WT (Table 1). The shift observed with steady-state inactivation was restored (Fig. 9*C-d*), with a slight shift to more negative voltages. The time constant of recovery from inactivation was not statistically different from the WT and the R130C mutant (Fig. 9*C-e*, and Table 1 for τ_{rec} values).

Since R117 K did not generate any current, we have investigated whether R117C labelled with MTSET, a positively charged cysteine reagent, could mimic WT-type gating properties. TsA201 cells transfected with R117C NaChBac mutant channel were either treated with 0.5 mM MTSET to assess the effect of the extracellular application of the reagent or applied in the patch pipette to assess its effect from the intracellular side. Figure 10 shows the effect on whole-cell Na^+ currents of MTSET applied in the patch pipette (*Intracellular*) (Fig. 10*B-a*) and

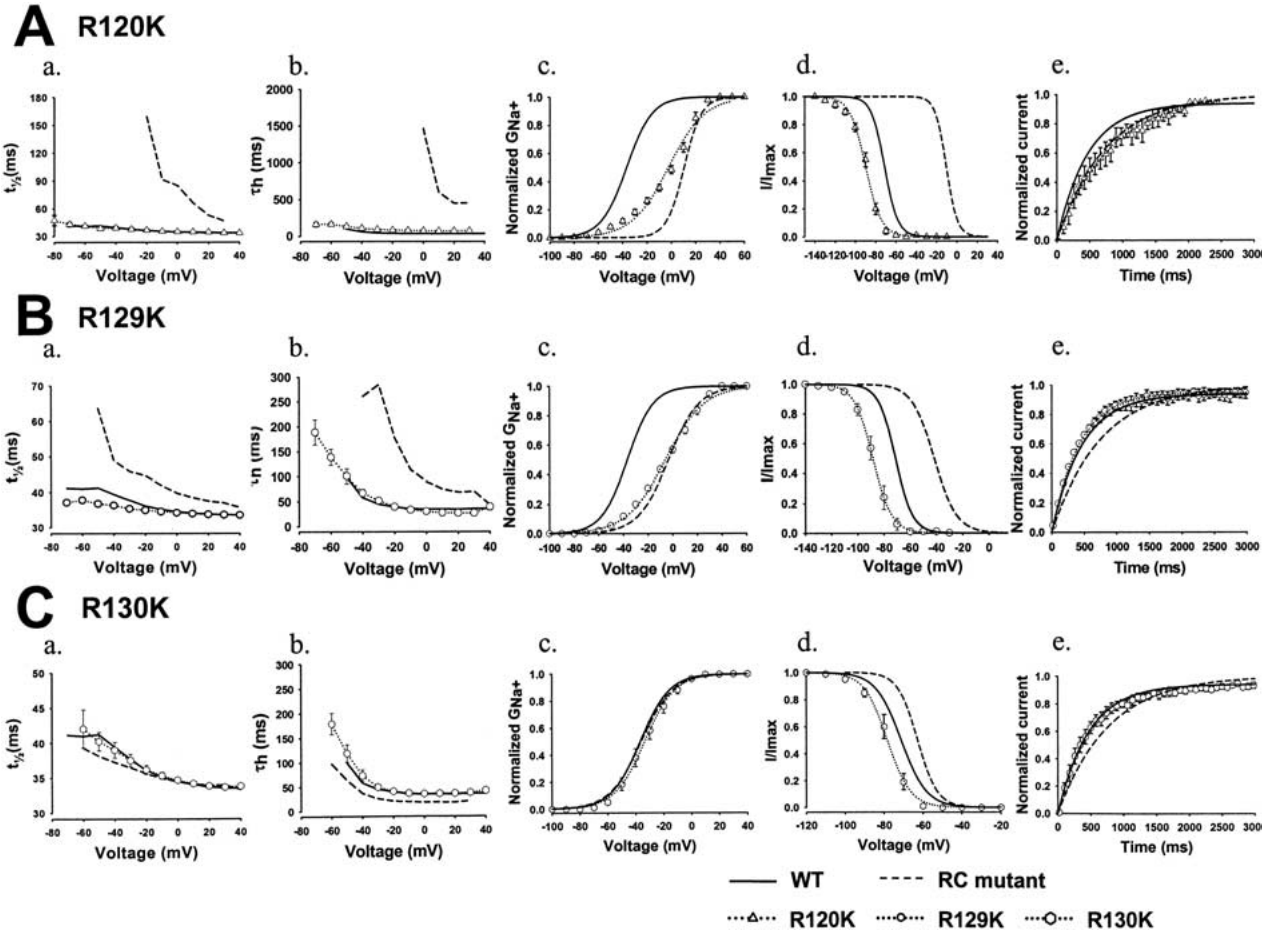

Fig. 9. Effects of conservation of S4 charges (R120K, R129K and R130K) on sodium-current activation and inactivation kinetics, steady-state activation (*G-V*) and inactivation h_∞ and recovery from inactivation. Voltage dependence of the time constants of $t_{1/2}$ of activation (*A,-a B,-a* and *C-a* for R120K, R129K and R130K respectively), voltage dependence of time constants of inactivation (τ_h) (*A,-b, B-b* and *C-b* for R120K, R129K and R130K, respectively), normalized conductance versus voltage (*G-V*) (*A-c, B-c* and *C-c* for R120K, R129K and R130K, respectively), steady-state availability (h_∞) (*A-d, B-d*, and *C-d* for R120K, R129K and R130K, respectively), and recovery from fast inactivation at a holding potential of −140 mV (*A-e, B-e* and *C-e* for R120K, R129K and R130K, respectively). For comparison, plots for WT and the corresponding cysteine mutants are shown on the same graphs. For *G-V* and h_∞, the symbols are normalized values and the lines are single Boltzmann fits to the data points.

applied in the bath (*Extracellular*) (Fig. 10*B-b*) compared to the control (Fig. 10*A-a*, dotted line) without MTSET treatment. When MTSET was applied in the patch pipette dramatic changes in current kinetics (Fig. 10*A-b*) and shift of 50 mV of activation curve (Fig. 10*B-a*) were observed ($V_{1/2}$ = 23.17 ± 2.93 mV, k_v = 6.57 ± 0 88 mV, n = 5 versus $V_{1/2}$ = −32.53 ± 1.53 mV, k_v = 10.52 ± 0.7 mV, n = 8 for R117C without MTSET, Table 1). No obvious alterations were observed when MTSET was applied in the bath (Fig. 10*A-c* and *B-b*). The MTSET reactivity was not state-dependent, since in high K^+ extracellular application of MTSET did not affect the gating properties of R117C (*see* Fig. 10*B-c* for effects on the activation curve). No significant effects on WT channels were observed when MTSET was applied from either intra- or extracellular space (*data not shown*).

Discussion

The S4 segment of the NaChBac channel has positively charged arginine residues every third position along the proposed α-helical structure and is believed to act as the voltage sensor of the channel. The close homology between NaChBac and the recently crystallized KvAP potassium channel suggests that the S4 of NaChBac is likely to play a similar voltage-sensing role as the S4 of Kv-type channels (Jiang et al., 2003a,b). In this study, we investigated the effect of S4 segment charge neutralization on the kinetics and voltage-dependent gating of NaChBac expressed in tsA201 cells. With the exception of the R117 K mutant and the R111C-R114C double mutant, for which we obtained reduced expression levels, heterologous expression of the S4 mutations resulted in large currents, indicating that substitutions at these positions

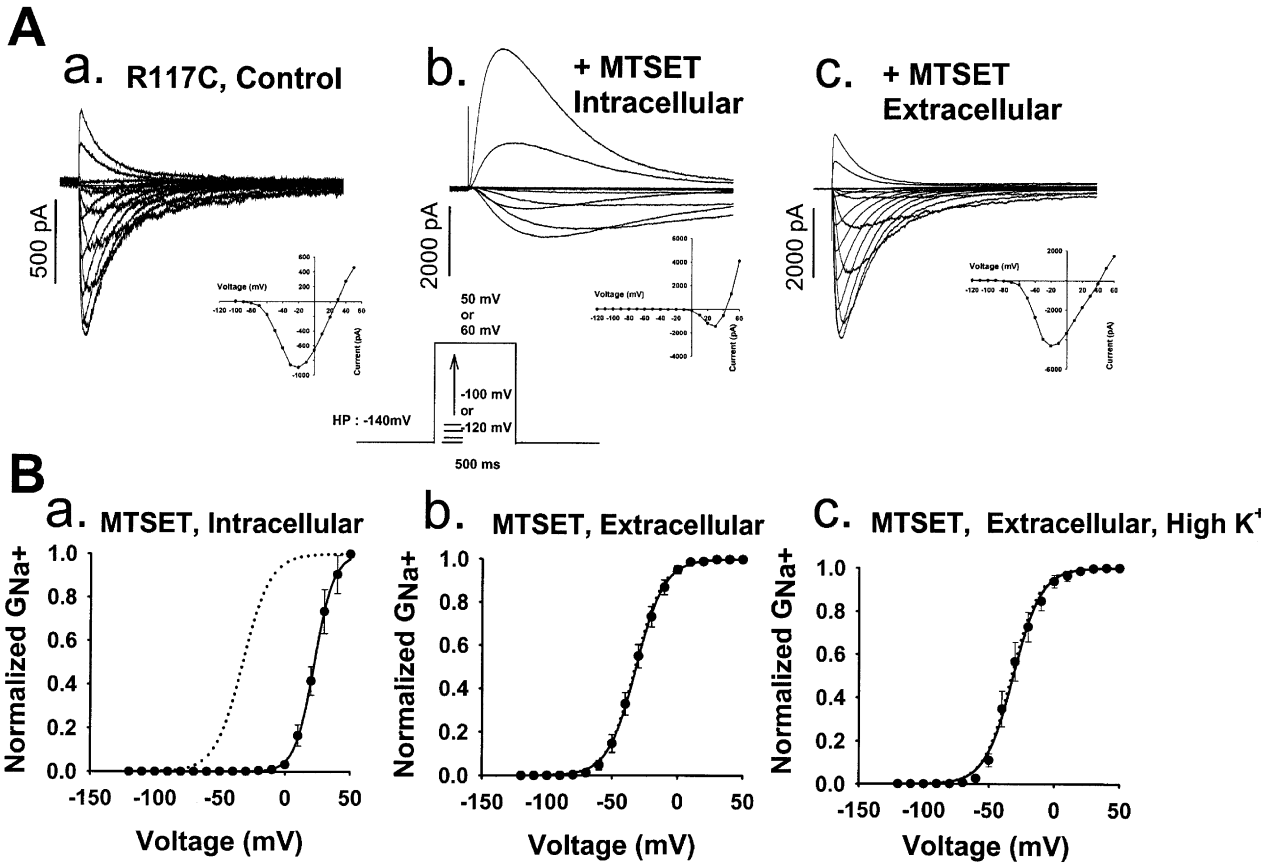

Fig. 10. Effect of extracellular or intracellular application of MTSET on R117C mutant channel. *Upper panels* (*A*) are representative current traces showing the effect of MTSET exposure of R117C (*A-b* and *A-c*) compared to the control (*A-a*). Na^+ currents were evoked by 4 s depolarizing pulses (only 500 ms are shown) starting at –120 mV in 10 mV increments. Lower panels (*B*) show *G-V* curve of MTSET applied from the intracellular (*B-a*) and extracellular (*B-b*) side. Panel *B-c* shows the effect of MTSET applied from the extracellular side when the transfected tsA201 cells were depolarized to zero mV with high K^+. The dotted lines represent fits obtained with R117C without MTSET.

are generally well tolerated by the channel. All the expressed currents reversed at the predicted sodium reversal potential, indicating that the S4 mutations did not alter the selectivity of the channel. The effects of the S4 mutations on the midpoint and voltage sensitivity of activation and inactivation and the kinetics of channel gating were investigated.

S4 Mutations Alter the Voltage Dependence of NaChBac Activation

Reductions in the slope were consistent with the S4 segment acting as a voltage sensor. Neutralizing positively charged residues at positions 111 and 114 were consistent with these residues acting as key players in sensing voltage. The *z* values were significantly reduced with charge neutralization of R111 and R114, suggesting that these two outermost positive charges play a special role in voltage sensing. Paradoxically, one of the arginine substitutions (R120C) caused an increase in the slope factor (increased *z* value), a result that is inconsistent with an important role for this residue in voltage sensing. Mutations at this position may alter the distance that S4 moves into the membrane electric field. Either R120C allows more of the S4 charge to enter the electric field or the same number of charges traverse a greater fraction of the field. However, the majority of the S4 mutants displayed shifts in the midpoint and reductions in the slope of the steady-state activation that were consistent with the S4 segment acting as a voltage sensor (Table 1).

The activation of the R111C/R129C double mutation was best fitted by a double Boltzmann equation. The combined effects of these mutants on activation were not additive, suggesting that either R129 is not part of the voltage sensor or that this residue acts separately from other arginine residues on the S4 segment. Steady-state inactivation of the R111C/R129C double mutant was shifted to more hyperpolarized voltages and fitted with only one Boltzmann function. This effect could be related to the fact that activation is a coordination of the movement of all S4 segments and, in inactivation, one

S4 segment dominates. The driving force for the large shift might largely originate from the very slow recovery from inactivation observed with the double mutant.

S4 Mutations Alter the Kinetics of NaChBac Gating

The changes in the half-time of activation ($t_{1/2}$) correlated well with a charge neutralization of positive charges on the voltage sensor, except for the neutralization of the R residue at position 130, which had more rapid activation and inactivation kinetics.

Single neutralization of R114, R117 or R120 resulted in very slow recovery from inactivation when they were individually replaced with C. Furthermore, mutating R120 with K, a conservative charge, retained WT-like current kinetics but produced an intermediate *G-V* curve and shifted the steady-state inactivation to more hyperpolarized potentials. This indicates that the structure of the arginine at position 120 plays an important role in channel activation. Replacing R with K at position 130 retained WT-like gating properties, indicating that the positive charge at this position is required for normal gating of the NaChBac channel. Except for R130, charge conservation by substituting R with K did not fully restore the five parameters we studied. For example, the presence of a positive charge at position 120 was essential for obtaining WT-like kinetics of activation and inactivation, but the *G-V* curve was intermediate between WT and R120C. In addition, h_∞ was shifted to more hyperpolarized voltages and the recovery from inactivation was the same as for the R120C mutant. This highlights the importance of the nature of the amino acid at this specific location in achieving normal channel gating properties.

Our results suggest that the positively charged residues on the S4 segment are also involved in fast inactivation. Mutating the R130 residue to either cysteine or lysine (a conservative charge) resulted in dramatic changes in inactivation kinetics. This indicates that this residue may play an important role in the inactivation process. Although the inactivation gate of the NaChBac channel is not known, our data suggest that the arginine residue at position 130 plays an important role in this process. Further studies are required to identify the residues that constitute the region responsible for inactivation.

Since R117 K did not express measurable currents, we tested the effect of MTSET, a positively charged methanethiosulfonate derivative, which is a selective thiol-reactive compound. Our data show that MTSET modification of cysteine introduced at position 117, the third positively charged residue on NaChBac channel resulted in slow inactivation kinetics and a shift of the *G-V* curve of about 50 mV. MTSET reacted only when applied from the intracellular side, as evidenced by an important slowing of gating kinetics and a shift of the activation curve. This reactivity was not state-dependent since in high K^+, which depolarizes the membrane to zero mV, MTSET did not affect the gating properties of R117C mutant. This suggested that R117C is buried in the membrane or in the channel protein and that the presence of a positive charge at this position is not sufficient to mimic WT-like channel gating properties. Other experiments are required to test the role and state-dependence of other charged MTS reagents and their accessibility.

In conclusion, the S4 segment of the NaChBac channel most probably acts as the voltage sensor, while the charged amino-acid residues in this region contribute to the changes in the gating charge movement of this channel. Overall, our data support the notion that conserved arginine residues of the S4 segment are important determinants of NaChBac voltage sensing.

This study was supported by grants from the Heart and Stroke Foundation of Quebec (HSFQ) and the Canadian Institutes of Health Research (CIHR) MT-13181 and the Japan New Energy and Industrial Technology Development Organization (NEDO). Dr. M. Chahine is an Edwards senior investigator (Joseph C. Edwards Foundation). The authors are grateful to Dr. L. Gailis and Dr. R Horn for their comments on the manuscript.

References

Armstrong, C.M., Hille, B. 1998. Voltage-gated ion channels and electrical excitability. *Neuron* **20:**371–380

Catterall, W.A. 1986. Molecular properties of voltage-sensitive sodium channels. *Annu. Rev. Biochem.* **55:**953–985

Catterall, W.A. 1992. Cellular and molecular biology of voltage-gated sodium channels. *Physiol. Rev.* **72:**S15–S48

Catterall, W.A. 2000. From ionic currents to molecular mechanisms: the structure and function of voltage-gated sodium channels. *Neuron* **26:**13–25

Cha, A., Bezanilla, F. 1997. Characterizing voltage-dependent conformational changes in the *Shaker* K^+ channel with fluorescence. *Neuron* **19:**1127–1140

Cha, A., Snyder, G.E., Selvin, P.R., Bezanilla, F. 1999. Atomic scale movement of the voltage-sensing region in a potassium channel measured via spectroscopy. *Nature* **402:**809–813

Chahine, M., George, A.L., Zhou, M., Ji, S., Sun, W., Barchi, R.L., Horn, R. 1994. Sodium channel mutations in para myotonia congenita uncouple inactivation from activation. *Neuron* **12:** 281–294

Chanda, B., Bezanilla, F. 2002. Tracking voltage-dependent conformational changes in skeletal muscle sodium channel during activation. *J. Gen. Physiol.* **120:**629–645

Fozzard, H.A., Hanck, D.A. 1996. Structure and function of voltage-dependent sodium channels: comparison of brain II and cardiac isoforms. *Physiol. Rev.* **76:**887–926

Glauner, K.S., Mannuzzu, L.M., Gandhi, C.S., Isacoff, E.Y. 1999. Spectroscopic mapping of voltage sensor movement in the Shaker potassium channel. *Nature* **402:**813–817

Goldin, A.L. 2002. Evolution of voltage-gated Na^+ channels. *J. Exp. Biol.* **205:**575–584

Gonzalez, C., Rosenman, E., Bezanilla, F., Alvarez, O., Latorre, R. 2001. Periodic perturbations in *Shaker* K^+ channel gating

kinetics by deletions in the S3-S4 linker. *Proc. Natl. Acad. Sci. USA* **98:**9617–9623

Guy, H.R., Seetharamulu, P. 1986. Molecular model of the action potential sodium channel. *Proc. Natl. Acad. Sci. USA* **83:**508–512

Hamill, O.P., Marty, A., Neher, E., Sakmann, B., Sigworth, F.J. 1981. Improved patch-clamp techniques for high-resolution current recording from cells and cell-free membrane patches. *Pfluegers Arch.* **391:**85–100

Hille, B. 2001. Ionic channels of excitable membranes. Sinauer Associates, Sunderland, MA,

Hodgkin, A.L., Huxley, A.F., Katz, B. 1952. Measurement of current-voltage relations in the membrane of the giant axon of Loligo. *J. Physiol.* **116:**424–448

Jiang, Y., Lee, A., Chen, J., Ruta, V., Cadene, M., Chait, B.T., MacKinnon, R. 2003a. X-ray structure of a voltage-dependent K^+ channel. *Nature* **423:**33–41

Jiang, Y., Ruta, V., Chen, J., Lee, A., MacKinnon, R. 2003b. The principle of gating charge movement in a voltage-dependent K^+ channel. *Nature* **423:**42–48

Jurman, M.E., Boland, L.M., Liu, Y., Yellen, G. 1994. Visual identification of individual transfected cells for electrophysiology using antibody-coated beads. *Biotechniques* **17:**876–881

Lainé, M., Lin, M.C.A., Bannister, J.P.A., Silverman, W.R., Mock, A.F., Roux, B., Papazian, D.M. 2003. Atomic proximity between S4 segment and pore domain in Shaker potassium channels. *Neuron* **39:**467–481

Liman, E.R., Hess, P., Weaver, F., Koren, G. 1991. Voltage-sensing residues in the S4 region of a mammalian K^+ channel. *Nature* **353:**752–756

Margolskee, R.F., McHendry-Rinde, B., Horn, R. 1993. Panning transfected cells for electrophysiological studies. *Biotechniques* **15:**906–911

Noda, M., Ikeda, T., Suzuki, H., Takeshima, H., Takahashi, T., Kuno, M., Numa, S. 1986. Expression of functional sodium channels from cloned cDNA. *Nature* **322:**826–828

Papazian, D.M., Timpe, L.C., Jan, Y.N., Jan, L.Y. 1991. Alteration of voltage-dependence of *Shaker* potassium channel by mutations in the S4 sequence. *Nature* **349:**305–310

Ren, D., Navarro, B., Xu, H., Yue, L., Shi, Q., Clapham, D.E. 2001. A prokaryotic voltage-gated sodium channel. *Science* **294:**2372–2375

Ren, D., Yue, L., Navarro, B., Ramos, A., Clapham, D.E. 2003. The cation selectivity filter of the one-repeat voltage-gated sodium channel, NaChBac. *Biophys. J.* **84:**24a

Strong, M., Chandy, K.G., Gutman, G.A. 1993. Molecular evolution of voltage-sensitive ion channel genes: on the origins of electrical excitability. *Mol. Biol. Evol.* **10:**221–242

Stühmer, W., Conti, F., Suzuki, H., Wang, X.D., Noda, M., Yahagi, N., Kubo, H., Numa, S. 1989. Structural parts involved in activation and inactivation of the sodium channel. *Nature* **339:**597–603

Takami, H., Nakasone, K., Ogasawara, N., Hirama, C., Nakamura, Y., Masui, N., Fuji, F., Takaki, Y., Inoue, A., Horikoshi, K. 1999. Sequencing of three lambda clones from the genome of alkaliphilic *Bacillus* sp. strain C-l25. *Extremophiles* **3:**29–34

Takami, H., Nakasone, K., Takaki, Y., Maeno, G., Sasaki, R., Masui, N., Fuji, F., Hirama, C., Nakamura, Y., Ogasawara, N., Kuhara, S., Horikoshi, K. 2000. Complete genome sequence of the alkaliphilic bacterium *Bacillus halodurans* and genomic sequence comparison with *Bacillus subtilis*. *Nucleic Acids Res.* **28:**4317–4331

Yang, N., George, A.L. Jr., Horn R. 1996. Molecular basis of charge movement in voltage-gated sodium channels. *Neuron* **16:**113–122

Yang, N.B., Horn, R. 1995. Evidence for voltage-dependent S4 movement in sodium channels. *Neuron* **15:**213–218